Supplementary Information: Short-term evolution of a supraglacial ice cliff in the Indian Himalaya

Pawan SINGH,[1] * Saurabh VIJAY,[1] Argha BANERJEE,[2] Chandan SARANGI,[3] Irfan RASHID[4]

[1]Civil Engineering Department, Indian Institute of Technology Roorkee, Roorkee, India,[2] Earth and Climate Science, Indian Institute of Science Education and Research, Pune, India, [3]Department of Civil Engineering, Indian Institute of Technology Madras, Chennai, India, [4] Department of Geoinformatics, University of Kashmir, Srinagar, India

Correspondence: Pawan Singh <pawansingh1610@gmail.com>

1. ENERGY BALANCE MODEL

The applied energy balance model in this paper is adapted from Han and others (2010), considering the net heat flux Q_m available for ice cliff melting (W m^{-2}):

$$Q_m = I_n + L_n + H + LE \tag{S1}$$

where I_n, L_n, H, LE are net shortwave (W m^{-2}), net longwave (W m^{-2}), turbulent sensible heat (W m^{-2}) and latent heat fluxes (W m^{-2}), respectively. The net shortwave radiation on an ice cliff slope in a unit-sloped area is given by:

$$I_n = (I_s + D_s + D_t)(1 - \alpha) \tag{S2}$$

where I_s, D_s, D_t and α are direct solar irradiance from the sky (W m^{-2}), diffused sky irradiance (W m^{-2}), diffuse irradiance (W m^{-2}) from surrounding terrain and the albedo of the ice cliff, respectively.

*

We used an Apogee pyranometer (SP-510 & SP-610) for incoming global solar radiation measurements on 30 June 2022 (Table S1). Albedo measurements were obtained using a SVC HR768i spectroradiometer on the ice cliff. We recorded two albedo measurements at 1430 hours and 1745 hours on 29 June 2023 to assess albedo's temporal variation and application to the model. The recorded values were 0.060 and 0.076, respectively. As the albedo's variation was not substantial, we considered an average albedo value of 0.07 for further calculation in the model.

The variation in direct solar irradiance (I_s) is influenced by the solar angle (sun position), specifically the solar incidence angle (θ), which is locally determined (Figure S1). Solar incidence angle is linked to the angle of slope (β) and azimuth (Z_s) of the ice cliff, as well as factors such as the sun's declination angle (δ), the latitude of the ice cliff (L), the Hour angle (h), and the horizon angle in the direction of the solar beam (H_s) all in degree (^{o}) (equation S3) (Garnier and Ohmura, 1968; Kalogirou, 2009; Wu and others, 2007).

$$\begin{aligned}\cos(\theta) = {} & \sin(L)\sin(\delta)\cos(\beta)\cos(L)\sin(\delta)\sin(\beta)\cos(Z_s) \\ & + \cos(L)\cos(\delta)\cos(h)\cos(\beta) + \sin(L)\cos(\delta)\cos(h)\sin(\beta)\cos(Z_s) \\ & + \cos(\delta)\sin(h)\sin(\beta)\sin(Z_s)\end{aligned} \tag{S3}$$

The relationship between direct solar irradiance (I_s) and direct normal irradiance (I_b) is shown in equation (S4), which is part of extraterrestrial radiation penetrating the atmosphere and solar incidence angle (θ).

$$I_s = \begin{cases} I_b\cos(\theta) & \text{if } \theta \leqslant H_s \\ 0 & \text{if } \theta > H_s \end{cases} \tag{S4}$$

The Horizon angle (H_s) is defined as the angle (^{o}) subtended by the line extending from a point to zenith and to the summit of the surrounding terrain in a given direction. To separate the element of diffused radiation from radiation observation, we follow the approach as in equations (S5) to (S11).

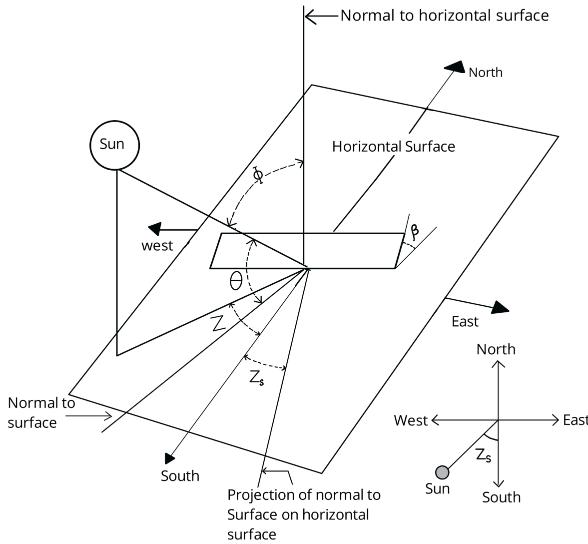

Figure S1. Solar angle Diagram

Table S1. Local Indian Standard Time (IST) with Hourly Mean Global Solar Incoming Radiation Measured by Pyranometer.

Indian Standard Time	Hourly mean global solar incoming radiation (W m^{-2})
1000 hours	670.2
1100 hours	773.15
1200 hours	825.18
1300 hours	762.22
1400 hours	736
1500 hours	710
1600 hours	685
1700 hours	660
1800 hours	635

$$I_b = \frac{I_o - D_h}{\sin(h)} \tag{S5}$$

$$D_h = k_d I_o \tag{S6}$$

$$k_t = \frac{I_o}{I_E} \tag{S7}$$

$$k_d = \begin{cases} 1.02 - 0.254k_t + 0.0123\sin(h) & \text{for } k_t \leqslant 0.3 \\ 1.4 - 1.749k_t + 0.177\sin(h) & \text{for } 0.3 < k_t \leqslant 0.78 \\ 0.486 - 0.182\sin(h) & \text{for } k_t \geqslant 0.78 \end{cases} \tag{S8}$$

$$I_E = E_o I_{sc} \sin(h) \tag{S9}$$

$$D_s = V_d D_h \tag{S10}$$

$$D_t = \alpha_t I_o (1 - V_d) \tag{S11}$$

I_b is the direct normal irradiance (W m^{-2}), I_o is the observed global radiation (W m^{-2}), D_h is the diffuse irradiance (W m^{-2}), and h is the solar elevation angle (^{o}), k_d is diffused fraction (dimensionless), k_t is clearness index (dimensionless), I_E is extraterrestrial radiation (W m^{-2}), I_{sc} is a solar constant taken as 1367 W m^{-2}. E_o is the eccentricity correction factor (dimensionless) of earth's orbit (Wong and Chow, 2001). D_s represents the diffuse sky irradiance while V_d corresponds to the sky view factor specific to a given ice cliff (it accounts for a portion of open sky visible to the ice cliff) (Steiner and others, 2015), which needs computation based on the horizon angle. D_t signifies the shortwave radiation received from the terrain reflection, and α_t represents the terrain albedo (taken as 0.24 from Han and others (2010)).

The net longwave radiation (L_n) can be split into L_s the incoming atmospheric longwave irradiance from unobscured portions of the sky (W m^{-2}), L_t the longwave irradiance from surrounding terrain (W m^{-2}), and L_o is the outgoing longwave irradiance (W m^{-2}), as shown in equation (Equation S12) and L_s is

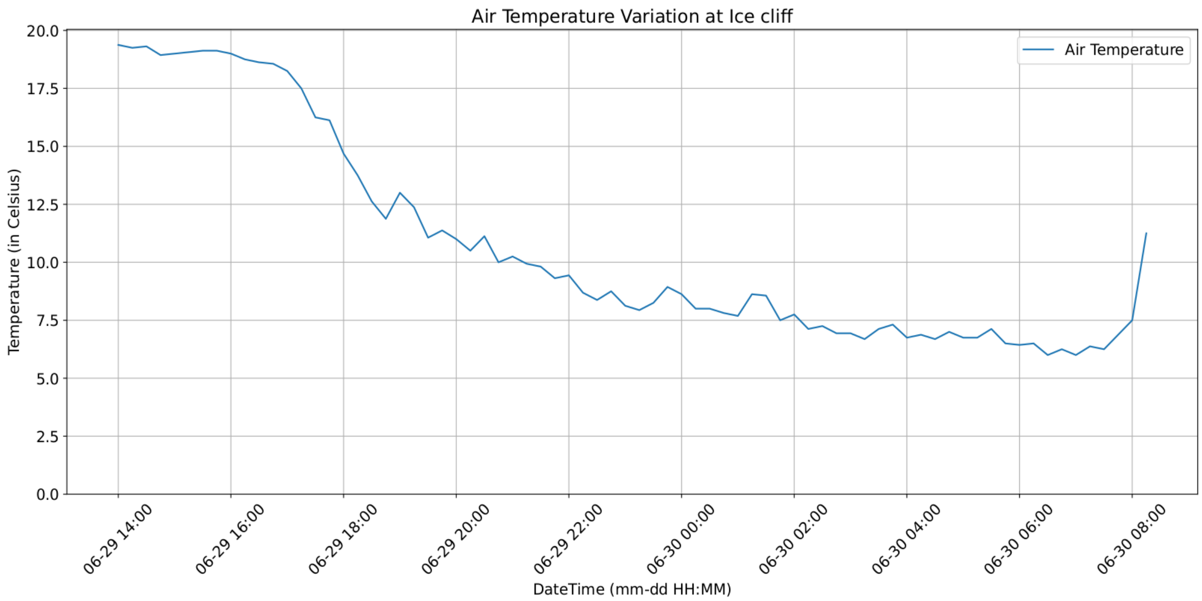

Figure S2. Temperature variation of surface and air temperatures from 29 June 2022, 13:30 IST to 30 June 2022, 09:30 IST, showing observed data points (every 15 minutes). Surface temperature fluctuates between 14°C and 3°C, while air temperature ranges from 6°C to 19°C.

obtained using the following equation (S13):

$$L_n = L_s + L_t - L_o \tag{S12}$$

$$L_s = V_d \left[1.31 \left(\frac{10 e_a}{T_a} \right)^{\frac{1}{7}} \sigma (T_a + 273.15)^4 \right] \tag{S13}$$

where σ is the Stefan Boltzmann constant (5.67 x 10^{-8} W m^{-2} k^{-4}), and e_a and T_a are the vapour pressure kPa and air temperature (in ^{o}C), respectively. we used the air (15 cm above the surface) temperature observed close to the ice cliff using Tomst TMS-4 temperature logger from 29 June 1330 hrs to 30 June 0945 hours (Figure S2). Since ground surface temperatures were also not available, the longwave irradiance from surrounding topography can be adequately computed assuming the ground radiates as a black-body radiator at screen air temperature (Cole, 1979). The longwave radiation emitted by terrain can be calculated using equation (S14), while an outgoing longwave from an ice cliff surface is calculated using equation (S15).

$$L_t = \sigma (T_a + 273.15)^4 (1 - V_d) \tag{S14}$$

$$L_o = \varepsilon\sigma(T_s + 273.15)^4 \tag{S15}$$

ε is the effective emissivity of the glacier, taken as 0.97, and T_s is the surface temperature of the ice cliff (^{o}C), assumed constant at 0 ^{o}C.(Han and others, 2010). Sensible H and latent heat LE fluxes are calculated using the bulk aerodynamic formula by (Sakai and others, 1998), as shown in equations (S16) and (S17).

$$H = 3.6U(T_a - T_s) \tag{S16}$$

$$LE = 2.31 \times 10^{-3} L_v U(e_a - e_s) \tag{S17}$$

where e_s is the vapor pressure of the ice surface and L_v is the latent heat of vaporization, and U is the wind speed. Finally, the Melt rate M can be estimated by:

$$M = \frac{Q_m}{\rho_{\text{ice}} L_f} \tag{S18}$$

where M is the melt rate (m sec^{-1}), ρ_{ice} is the density of ice (900 kg m^{-3}), L_f is the latent heat of fusion of ice (334 KJ kg^{-1}), and then using the slope of the ice cliff, we estimated the backwasting rate from the melt rate.

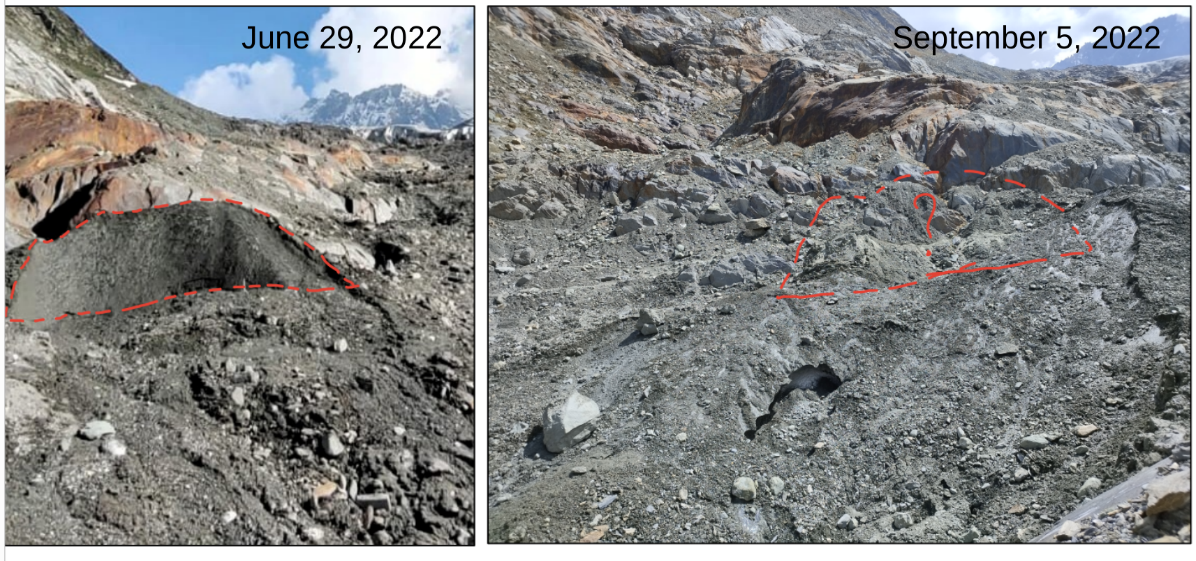

Figure S3. (Left) Field photograph of our observed ice cliff (red dashed line) and the same ice cliff later missing during field expedition during September (Right).

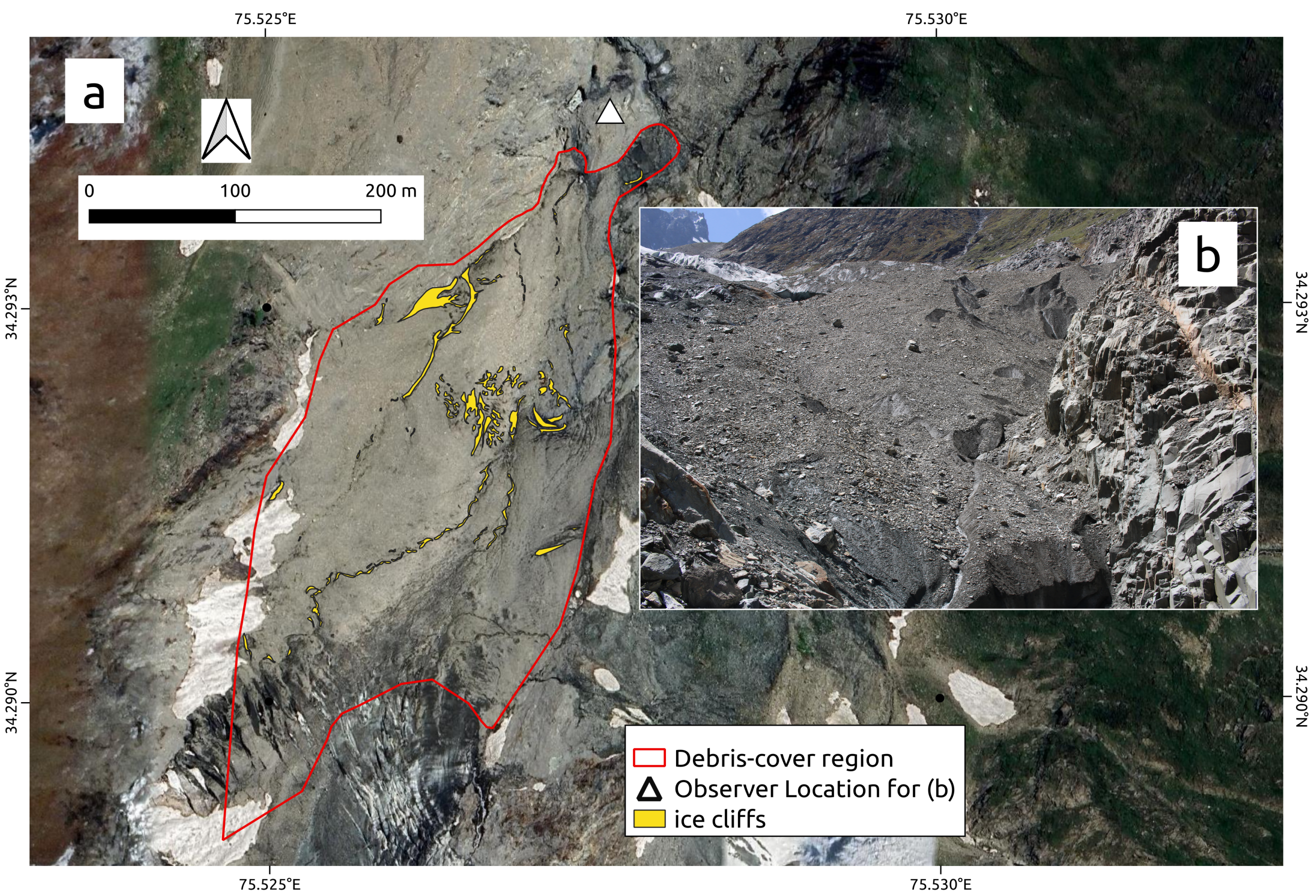

Figure S4. (a) Manually delineated ice cliff on the debris-covered part of the Machoi glacier using high-resolution Google satellite images from 7 July 2022. The approximate area covered by the delineated ice cliff was 2200 m^2. (b) Field photograph of the debris-covered part taken from stable bedrock near the terminus.

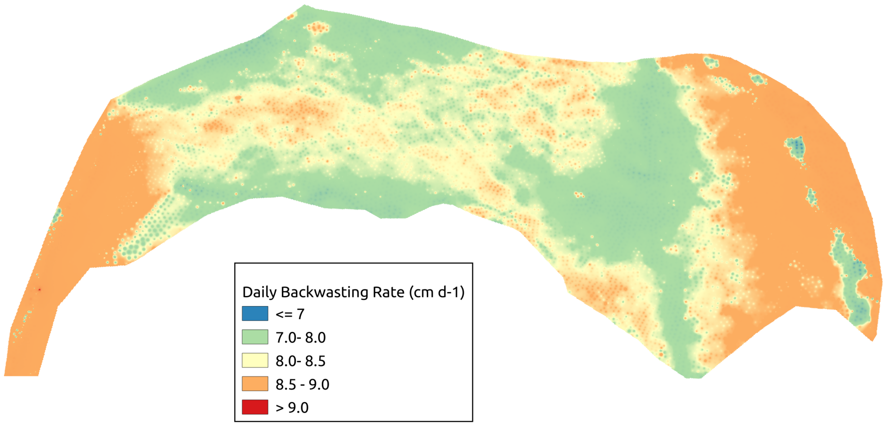

Figure S5. Mean daily backwasting rate of an ice cliff

Table S2. Observed mean backwasting rates derived from TLS point cloud data during different observation periods.

Observation Period	Mean Backwasting Rate (cm hr^{-1})
1630 hrs 28 June 2022 to 1430 hrs 29 June 2022	0.28
1430 hrs 29 June 2022 to 1530 hrs 29 June 2022	0.38
1530 hrs 29 June 2022 to 1630 hrs 29 June 2022	1.06
1630 hrs 29 June 2022 to 1730 hrs 29 June 2022	0.84
1730 hrs 29 June 2022 to 1830 hrs 29 June 2022	0.67
1430 hrs 29 June 2022 to 1630 hrs 29 June 2022	0.74
1630 hrs 28 June 2022 to 1630 hrs 29 June 2022	0.32 (7.7 cm d^{-1})
1830 hrs 29 June 2022 to 1250 hrs 30 June 2022	0.19
1630 hrs 28 June 2022 to 1250 hrs 30 June 2022	0.26

Table S3. Modelled and observed Mean Backwasting rate for All Zones of ice cliff (in cm hr^{-1})

Zone	Observation time	Modelled		Observed	
		Mean	Std Dev	Mean	Std Dev
Zone 1	1430 hrs to 1530 hrs	0.48	0.04	0.52	0.04
	1530 hrs to 1630 hrs	0.97	0.02	1.14	0.10
	1630 hrs to 1730 hrs	1.03	0.02	1.04	0.04
	1730 hrs to 1830 hrs	1.03	0.03	0.99	0.03
Zone 2	1430 hrs to 1530 hrs	0.53	0.05	0.47	0.05
	1530 hrs to 1630 hrs	0.86	0.02	0.83	0.10
	1630 hrs to 1730 hrs	0.95	0.02	0.88	0.04
	1730 hrs to 1830 hrs	1.02	0.02	0.83	0.03
Zone 3	1430 hrs to 1530 hrs	0.73	0.17	0.27	0.17
	1530 hrs to 1630 hrs	0.95	0.02	1.74	0.13
	1630 hrs to 1730 hrs	0.91	0.03	1.13	0.19
	1730 hrs to 1830 hrs	0.88	0.03	0.67	0.36

REFERENCES

Garnier BJ and Ohmura A (1968) A Method of Calculating the Direct Shortwave Radiation Income of Slopes. *Journal of Applied Meteorology*, **7**, 796–800 (doi: 10.1175/1520-0450(1968)007), aDS Bibcode: 1968JApMe...7..796G

Han H, Wang J, Wei J and Liu S (2010) Backwasting rate on debris-covered Koxkar glacier, Tuomuer mountain, China. *Journal of Glaciology*, **56**(196), 287–296 (doi: 10.3189/002214310791968430)

Kalogirou SA (2009) Environmental Characteristics. In *Solar Energy Engineering*, 49–762, Elsevier, ISBN 978-0-12-374501-9 (doi: 10.1016/B978-0-12-374501-9.00002-9)

Sakai A, masayoshi n and fujita k (1998) Melt rate of ice cliffs on the Lirung Glacier, Nepal Himalayas, 1996. *Bulletin of Glacier Research*, 57–66

Steiner JF, Pellicciotti F, Buri P, Miles ES, Immerzeel WW and Reid TD (2015) Modelling ice-cliff backwasting on a debris-covered glacier in the Nepalese Himalaya. *Journal of Glaciology*, **61**(229), 889–907 (doi: 10.3189/2015JoG14J194)

Wong L and Chow W (2001) Solar radiation model. *Applied Energy*, **69**(3), 191–224 (doi: 10.1016/S0306-2619(01)00012-5)

Wu G, Liu Y and Wang T (2007) Methods and strategy for modeling daily global solar radiation with measured meteorological data – A case study in Nanchang station, China. *Energy Conversion and Management*, **48**(9), 2447–2452 (doi: 10.1016/j.enconman.2007.04.011)